

# Enhancing Offshore Wind Integration by Integrated Electricity and Gas Systems With Hydrogen Blending

**Abstract**—The offshore wind farm is a pivotal generation component in the decarbonization of energy systems. However, their large capacity and inherent uncertainty pose great challenges for smooth integration into current electricity systems. This paper proposes an innovative offshore wind accommodation scheme employing integrated electricity and gas systems along with hydrogen blending techniques. Firstly, an uncertainty model for OWF generation is proposed considering the cumulative wake effect, where a recursive-tree-based method is used to improve the modelling efficiency. Then, a distributionally robust chance-constrained operation scheme of hydrogen-blended integrated electricity and gas systems is proposed, to regulate the gas system safety with stochastic hydrogen injection from offshore wind via power-to-gas, as well as variant gas compositions across the gas network. Gas security is modelled as chance constraints for aligning with practical gas safety regulations. To address the highly nonconvex distributionally robust chance-constrained optimization problem, a new unified affine policy is developed to handle high-order nonlinearities. Sequential convex programming is tailored and embedded in the distributionally robust chance-constrained solution procedure for handling various forms of nonlinearities. Finally, a practical large-scale Ireland Island energy system is used for validation. Our results indicate a remarkable improvement of 156.8% in offshore wind accommodation and 64.44% in carbon emission mitigation with the proposed operation strategy. This underscores the crucial role of hydrogen integration in meeting Ireland's decarbonization ambitions by 2050.

**Index Terms**—offshore wind, hydrogen, integrated power and gas systems, gas security, power to gas

## I. INTRODUCTION

OFF-SHORE wind farm (OWF) has gained rapid development in recent years as a promising solution towards net zero energy systems. Compared with onshore wind farms, the OWF usually has an abundant wind endowment and less influence on/from surrounding communities. By the end of 2022, the total installation capacity of OWF reached 63.2 GW, marking a tenfold increase over the past decades [1]. Many countries have shown their continuous commitment to OWF developments. For instance, the Irish government ambitiously aims to install 5 GW of offshore wind generation by 2030, and this number will continue to grow to contribute to the government's wider objectives of achieving 80 % renewable electricity and a 51% greenhouse gas emission by the end of this decade [2].

The rapid growth of OWF capacity poses great challenges to current electricity systems in terms of integration and accommodation issues. The substantial capacity and centralised installation of OWFs require for large capacities and robustness in on-shore distribution and transmission networks, especially near interconnection points. Moreover, the stochastic nature of wind requires more electricity system flexibility to ensure real-time balanced operation. Some previous research

efforts have been dedicated to addressing the OWF integration and operation challenges. For instance, a stochastic optimal operation model of power systems is developed in [3] for the integration of fluctuated OWFs. A probabilistic power flow model is developed in [4] to detect potential over-limit risks in advance for system operators with a high penetration of offshore wind. The OWF layout design and micrositing are investigated in [5]–[8] considering the wake effect. The development potential, grid interconnection feasibility, and levelized cost of electricity of the offshore wind in China coast areas are comprehensively studied in [9].

However, existing research focuses on addressing OWF uncertainties solely through electricity system flexibility, without exploring alternative options. While effective for the current OWF capacity, this approach may be insufficient as OWF capacity expands significantly in the long term. The ever-increasing focus on hydrogen offers an alternative promising solution to this problem. In addition to transporting OWF generation by electricity network, the surplus generation can also be channelled to produce hydrogen through power-to-gas (PTG) facilities. The produced hydrogen can be used on-site, or injected into existing gas pipelines, blended with natural gas, and distributed across the gas network. This hydrogen blending technology, exemplified by initiatives like HyDeploy [10] in the UK and HyBlend [11] in the US, is considered an effective measure for decarbonizing the energy system. By this means, the electricity and gas systems can be coordinated to expand the flexibility to accommodate large-scale stochastic offshore wind more effectively.

Utilizing the joint flexibility of both electricity and gas systems through hydrogen blending techniques (also known as hydrogen-blended electricity and gas systems (H-IEGS)) to accommodate stochastic and substantial volumes of offshore wind requires sophisticated operation strategies, which have not been studied before. The challenges mainly are twofold: 1) The substantial injection of hydrogen into the gas network due to the significant volume of offshore wind generation can fundamentally alter the physical properties of gas mixtures, such as a decrease in gross calorific values (GCV). As a result, the gas flow pattern across the network will change substantially because the residential, commercial, etc., energy users, as well as gas-fired power plants, will require larger volumes of gas mixtures to meet their gas demands. Moreover, hydrogen blending could introduce potential security issues like unideal combustion, hydrogen embrittlement, etc., adversely affecting the durability and lifespan of the gas systems components (including gas appliances, pipelines, etc.). Therefore, it is imperative to design more careful operation strategies. 2) The highly fluctuating OWF generations induce uncertain and variant gas compositions within the network. Compared with

the traditional mathematical model of the gas system, the H-IEGS optimization model faces more complex forms of nonconvexities (such as new Weymouth equations, gas mixing equations, etc.), which makes the solution intractable. The computation burden may further be amplified if advanced uncertainty-hedging operation strategies such as stochastic or robust optimization are adopted.

Recently, some emerging studies have made attempts in H-IEGS operation. For example, the optimal operation framework of H-IEGS is firstly developed in [12]. The probabilistic energy flow model of mixed hydrogen and natural gas is also developed in [13]. Multiple gas security constraints such as the Wobbe index are further considered in the optimization of H-IEGS in [14]. Advanced sequential programming method is developed for solving this optimization problem in [15]. The new linepack flexibility model with the injection of hydrogen in H-IEGS is quantified in [16], [17]. While these studies provide basic mathematical models for devising H-IEGS operation strategies, they target deterministic scenarios only. The uncertainties of large-scale OWFs can not be managed directly, and thus the aforementioned research gap still exists.

To this end, this paper proposes a novel offshore wind accommodation scheme by using the flexibility of both electricity/gas systems and hydrogen-blending techniques. The specific contributions are as follows:

- 1) A distributionally robust chance constrained (DRCC) operation framework is proposed for H-IEGS to accommodate large-scale stochastic OWF generation. Resulting from distributed and time-varying injection of hydrogen, variant gas composition and corresponding changeable physical properties (such as GCV, specific gravity, gas constant, etc.) are characterized to promote the accuracy of the DRCC model. Moreover, the gas-quality-related gas security indices are incorporated as chance constraints. Compared to the commonly used hard constraints [15], [17], [18], the modelling technique used in this paper is more in line with practical and recently updated gas safety regulations [19].
- 2) A sequential convex programming embedded DRCC (SCP-DRCC) solution method is tailored to reformulate the intractable DRCC optimization problems with various forms of nonconvexities into a second-order-cone programming form, so it can be solved by commercial solvers. Compared to the DRCC formulations of integrated electricity and gas systems in [20], [21], A new unified affine policy is also devised to enable the DRCC modelling with the presence of higher-order nonlinear equality constraints (such as Weymouth equation with variant gas constant).
- 3) The uncertainty of OWF is characterised as the moment-based ambiguity set based on historical data, where a recursive-tree-based method is developed to quantify the cumulative wake effects of wind turbines (WT). Compared to previous research [6]–[8] (which only considers a single layer of wake effect or uses enumeration-based methods for all WTs), the proposed one can achieve a better trade-off between accuracy and computation efficiency.

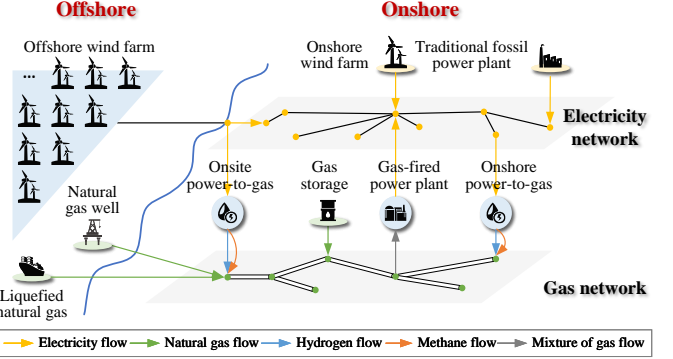


Fig. 1. Structure of OWF and H-IEGS

- 4) The offshore wind integration potential by hydrogen blending for the practical national energy systems on Ireland Island is comprehensively studied. Compared with using electricity system flexibility solely, we validate that the offshore wind accommodation rate is enhanced by 1.57 times if we can also coordinate the flexibility from the gas system and hydrogen blending. We have also identified barriers to offshore wind integration in Ireland, offering insights that could substantially benefit the government's decarbonization strategy in the long run.

## II. STRUCTURE OF OFFSHORE WIND AND H-IEGS

The structure of the studied energy system is shown in Fig. 1. The OWFs are connected to the onshore energy systems in two different ways – They can either be connected to the electricity systems directly through substations, or connected to PTGs. Then, the PTG consumes the surplus OWF generations to produce hydrogen or methane. These produced gas can be injected into natural gas pipelines, and then transported to distant locations for further use.

The onshore H-IEGS contains two layers, namely, gas network and electricity network. Apart from the gas production from PTGs, the gas system is mainly supplied by natural gas wells and seasonal gas storage. These gases with different compositions will be mixed, transported, and meet the gas demands. The electricity network is supplied by traditional fossil power plants, onshore wind farms, as well as gas-fired power plants which consume the gas mixtures from the gas network to generate electricity.

## III. UNCERTAINTY MODELING OF OFFSHORE WIND

To better operate the energy system against stochastic wind powers, the uncertainty of OWFs is firstly modelled. Compared to onshore wind, the wake effects can not be neglected. However, characterizing the cumulative wake effect among all WTs for continuous operation and numerous stochastic scenarios is extremely time-consuming. To address this issue, we developed a recursive-tree-based method to efficiently quantify the cumulative wake effect. The specific procedures are outlined in Fig. 2, and are also elaborated as follows:

**Step 1:** Model vectorized stochastic wind velocity. The electricity generation of OWFs depends on the stochastic wind

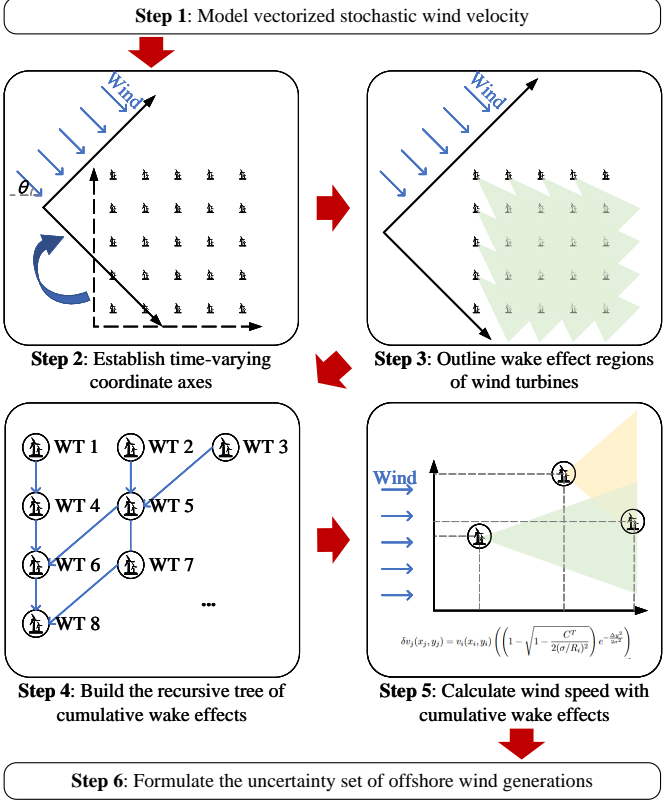


Fig. 2. Uncertainty modelling steps for dispatch capacity of OWFs considering cumulative wake effects.

velocity vector  $\dot{v}$ . It is described in two dimensions, speeds  $v$  and direction  $\theta$  (the angle between wind direction and parallel), each of which contains two parts, namely, forecast value ( $\bar{v}, \bar{\theta}$ ) and forecast deviation ( $\Delta v, \Delta \theta$ ):

$$\dot{v}_{m,k} = \{v_{m,k} = \bar{v}_{m,k} + \Delta v_{m,k}, \theta_{m,k} = \bar{\theta}_{m,k} + \Delta \theta_{m,k}\} \quad (1)$$

where  $m$  and  $k$  are indices for area and time period. In this paper, our wind velocity data are based on geographical coordinates, and thus the area here refers to particular segments within certain ranges of latitude and longitude.

**Step 2:** Establish time-varying coordinate axes according to the wind direction. For conveniently calculating the wake effect, the coordinate axis of the WT should be rotated during the operation with the change of wind direction. The new coordinates can be calculated by:

$$\begin{bmatrix} x_n \\ y_n \end{bmatrix} = \begin{bmatrix} \cos \theta & -\sin \theta \\ \sin \theta & \cos \theta \end{bmatrix} \begin{bmatrix} x_{n,0} \\ y_{n,0} \end{bmatrix} \quad (2)$$

where  $x_{n,0}$  and  $y_{n,0}$  are the geographical coordinates of WT  $n$ ;  $x_n$  and  $y_n$  are the new coordinates after rotation.

**Step 3:** Outline the wake effect regions of WTs. The wake effect refers to the phenomenon that the downstream wind speed of WTs could be affected and lowered by upstream WTs, and thus leading to the reduction of total electricity generation of the WT fleet. As shown in Fig. 3, using the Jensen-Gaussian wake model, the decrease in wind speed at location  $(x, y)$

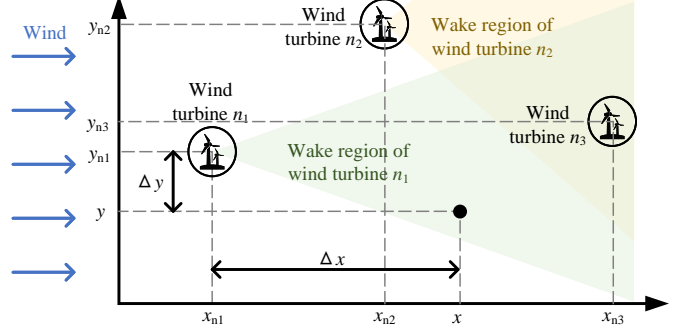


Fig. 3. Illustration for wake effect of offshore wind turbines

caused by the WT  $n_1$ ,  $\delta v_{n_1}$ , can be calculated as [6]:

$$\delta v_{n_1} = v_{n_1} \left( \left( 1 - \sqrt{1 - \frac{C^T}{2(\omega/R_{n_1})^2}} \right) e^{-\frac{\Delta y^2}{2\omega^2}} \right) \quad (3)$$

where  $v_{n_1}$  is the wind speed at the location of WT  $n_1$ ;  $C^T$  is the WT thrust coefficient;  $R_{n_1}$  is the rotor radius;  $\Delta y = |y - y_{n_1}|$  is the difference in latitude;  $\omega$  is the characteristic width of the wake, which is calculated by [6]:

$$\omega = (R_{n_1} + 0.56 / (\ln z^h - \ln z_0) \Delta x) / 2 \quad (4)$$

where  $z^h$  is the WT hub height, and  $z_0$  is the surface roughness length;  $\Delta x = x - x_{n_1}$ ,  $x \geq x_{n_1}$  is the difference in longitude. Observing from the above formulations, we notice that the wake effect decreases with the increase of  $x$  and  $y$ . Here we set a tolerance gap  $\epsilon^w$ , to outline the significant wake effect region of a WT by solving  $\delta v_{n_1} > \epsilon^w$ . We denote the solution for WT  $n$  as  $(x, y) \in \mathbb{W}_n$ . Since in most case the wind turbines are identical in a wind farm, it only need to be calculated once.

**Step 4:** Build the recursive tree of cumulative wake effects. Wake effect has cumulative effects. The decrease of wind speed from the wake effect of an upstream WT, will continue to have residual effect on the downstream ones. Besides, one WT could also be affected by multiple upstream WTs, as shown by the WT  $n_3$  in Fig. 3. Therefore, here we build a recursive tree, as shown in the step 4 of Fig. 2. For example, the coordinate for WT 4 is in the significant wake effect region of WT 1, i.e.,  $(x_4, y_4) \in \mathbb{W}_1$ , then, we claim WT 1 affects WT 4, and then we find all the co-relation among WTs.

**Step 5:** Calculate wind speed considering cumulative wake effects. As shown in the Fig. 3, the WT  $n_3$  is jointly affected by WT  $n_1$  and  $n_2$ . Generally, the wind speed of WT  $n$  can be calculated by:

$$v_n = v_m - \left( \sum_{n' \in \mathcal{N}_n} \delta v_{n'} \right)^{\frac{1}{2}} \quad (5)$$

where  $v_m$  is the original wind speed in area  $m$ ;  $\mathcal{N}_n$  is the set of WTs that affect WT  $n$ .

**Step 6:** Formulate the uncertainty set of offshore wind generations. After obtaining the wind speed at each WT locations, the available generating capacity OWF,  $P_{i,k}^{max,owf}$ , can be calculated as:

$$P_{i,k}^{max,owf} = \sum_{m \in \mathcal{M}_i} \sum_{n \in \mathcal{N}_{i,m}} f^{wt}(v_{n,k}) \quad (6)$$

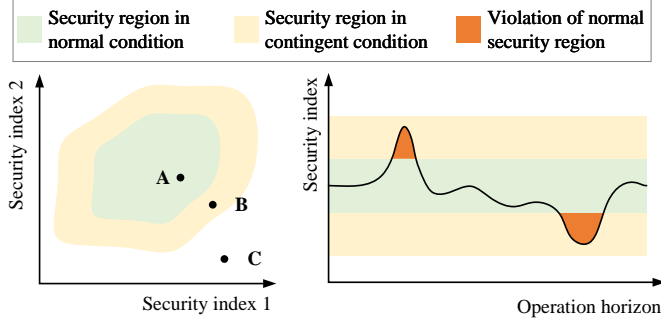


Fig. 4. Gas security budget.

where  $M_i$  is the set of areas at electricity bus  $i$ ;  $\mathcal{N}_{i,m}$  is the set of WTs in area  $m$  at bus  $i$ ;  $f(\cdot)^{wt}$  is the electricity generating function of WT with respect to wind speed [22].

After obtaining all the related prediction errors of available generating capacity from historical data, the moment-based ambiguity set of available generating capacity of OWFs,  $\Xi$ , can be expressed as:

$$\Xi_i = \left\{ \Pr(\xi) | \mathbb{E}(\xi) = \mu, \mathbb{E}(\xi\xi^T) = \sigma \right\} \quad (7)$$

where  $\xi$  is the set of prediction error for available generation capacities;  $\mathbb{E}(\cdot)$  represents expectation;  $\mu$  and  $\sigma$  are the mean value and variance of prediction errors.

#### IV. FORMULATION OF DRCC OPERATION OF H-IEGS

For accommodating the stochastic offshore wind, a DRCC operation framework for H-IEGS is developed in this section.

##### A. Gas security chance constraints

Due to the fluctuation of OWF generations, the hydrogen productions from PTGs and hydrogen injections to the pipelines are all time-varying. As a result, the hydrogen concentrations across the gas network also become variant. As discussed in the introduction, gas appliances and system components have requirements for gas composition to operate safely. This kind of requirement can be expressed as the gas security region, as shown in the left half of Fig. 4. It is outlined by a set of gas security indices, which varies by countries and regions. Here we adopt the indices used in the Gas Safety Management Regulation (2023 amendment) as an example [19], including Wobbe Index  $WI_{i,k}$ , relative density  $RD_{i,k}$ , etc. Additionally, to cope with the impacts of hydrogen on combustion dynamics, we further introduce flame speed factor  $FS_{i,k}$ . They are calculated as:

$$WI_{i,k} = \sum_{g \in \mathcal{G}} \chi_{i,k,g} GCV_g (RD_{i,k})^{-\frac{1}{2}} \quad (8)$$

$$RD_{i,k} = \sum_{g \in \mathcal{G}} \chi_{i,k,g} M_g / M^{air} \quad (9)$$

$$FS_{i,k} = \frac{\sum_{g \in \mathcal{G}} \chi_{i,k,g} f_{sg}}{AF + 5\chi_{i,k}^{ni} - 18.8\chi_{i,k}^{ox} + 1} \quad (10)$$

where  $g$  and  $\mathcal{G}$  are the index and set for gas components, respectively;  $\chi_{i,k,g}$  is the concentration of gas component  $g$  at

bus  $i$  in time period  $k$ ;  $\chi_{i,k}^{ni}$  and  $\chi_{i,k}^{ox}$  are the molar fractions of nitrogen and oxygen, respectively;  $GCV_g$  is the GCV of gas component  $g$ ;  $M_g$  is the molecular weight of gas component  $g$ ;  $M^{air}$  is the molecular weight of air;  $f_{sg}$  is the flame speed factor of gas component  $g$ ;  $AF$  is the air-fuel ratio.

Practically there are two gas security regions according to gas safety regulations, one is used in normal conditions, and the other is used only in contingencies, as marked by light green and yellow, respectively in Fig. 4. For example, for the three points , point A represents an acceptable gas composition, point B is acceptable in contingent states, while point C is unacceptable in any case. During the operation, with the fluctuation of wind, the security indices of the gas mixture will be time varying, and sometimes may violate the normal security regions, as marked in orange in the right half of Fig. 4. Following this idea, we model the normal and contingent security region as two sets of chance constraints with different risk thresholds,  $\epsilon^N$  and  $\epsilon^C$ , respectively (the constraints in normal state is presented here, and the constraints in contingent states can be written identically):

$$\inf_{\Xi} \Pr \left\{ WI^{min,N} \leq W\tilde{I}_{i,k} \leq WI^{max,N}, R\tilde{D}_{i,k} \leq RD^{max,N}, FS^{min,N} \leq F\tilde{S}_{i,k} \leq FS^{max,N} \right\} \geq 1 - \epsilon^N \quad (11)$$

where  $WI^{min,N}$ ,  $FS^{min,N}$ ,  $WI^{max,N}$ ,  $RD^{max,N}$ , and  $FS^{max,N}$  are the lower and upper bounds of Wobbe Index, relative density, and flame speed factor, in the normal state, respectively;  $(\cdot)$  means the affine mapping of variable  $(\cdot)$ . For example:

$$\tilde{WI}_{i,k} = WI_{i,k} + \varphi_{i,k}^{WI} (\mathbf{1}^T \xi_k) \quad (12)$$

where  $\varphi_{i,k}^{WI}$  is the adjustment factor of Wobbe index with respect to the wind forecast error.

##### B. Gas system model with variant gas compositions

Due to the time-varying hydrogen injections, the physical properties of the gas mixtures are transferred from originally stationary to variant. This substantially changed the ways in which gases are produced, transported, and consumed.

In the production stage, gases can come from gas wells, gas storages, PTGs, etc. They may have different gas compositions, which can be written as:

$$\tilde{q}_{i,l,k,g}^s = \chi_{i,l,g}^s \tilde{q}_{i,l,k}^s, \sum_{g \in \mathcal{G}} \chi_{i,l,g}^s = 1 \quad (13)$$

$$\inf_{\Xi} \Pr \left\{ q_{i,l}^{s,min} \leq \tilde{q}_{i,l,k}^s \leq q_{i,l}^{s,max} \right\} \geq 1 - \epsilon^G \quad (14)$$

$$\tilde{q}_{i,l,k}^{hy} GCV^{hy} + \tilde{q}_{i,l,k}^{me} GCV^{me} \eta_{i,l}^{me} = \tilde{P}_{i,l,k}^{ptg} \eta_{i,l}^{el} \quad (15)$$

$$\inf_{\Xi} \Pr \left\{ P_{i,l,k}^{ptg,min} \leq \tilde{P}_{i,l,k}^{ptg} \leq P_{i,l,k}^{ptg,max} \right\} \geq 1 - \epsilon^G \quad (16)$$

$$\inf_{\Xi} \Pr \left\{ \tilde{q}_{i,l,k}^{me}, \tilde{q}_{i,l,k}^{hy} \geq 0 \right\} \geq 1 - \epsilon^G \quad (17)$$

where  $\tilde{q}_{i,l,k}^s$  is the gas supply from gas source  $l$  at bus  $i$  at time period  $k$ ; More specifically,  $\tilde{q}_{i,l,k,g}^s$  is the gas supply

for gas component  $g$ ;  $\chi_{i,l,g}^s$  is the gas composition of gas component  $g$ ;  $q_{i,l}^{s,min}$  and  $q_{i,l}^{s,max}$  are the lower and upper limits for gas sources, respectively;  $\tilde{q}_{i,l,k}^{hy}$  and  $\tilde{q}_{i,l,k}^{me}$  are the hydrogen and methane productions of PTG, respectively;  $GCV^{hy}$  and  $GCV^{me}$  are the GCVs for hydrogen and methane, respectively;  $\eta_{i,l}^{el}$  and  $\eta_{i,l}^{me}$  are the efficiencies of electrolysis and methanation processes, respectively;  $\tilde{P}_{i,l,k}^{ptg}$  are the electricity consumption of PTG;  $P_{i,l,k}^{ptg,min}$  and  $P_{i,l,k}^{ptg,max}$  are the lower and upper bounds for PTG electricity consumptions, respectively.

The produced gases are transported through pipelines, which is governed by Weymouth equations as in (18). It is worth noting that different from the traditional natural gas system with consistent gas compositions, the physical properties (i.e., the gas constant) of the gas mixtures is a variant here. This will make the original Weymouth equations more nonconvex:

$$\tilde{p}_{i,k}^2 - \tilde{p}_{j,k}^2 = \gamma_{ij,k} \frac{16 f_{ij} (\rho^{ng})^2 T^{ng} L_{ij} z^{ng}}{\pi^2 D_{ij}^5} \tilde{r}_{ij,k} \tilde{q}_{ij,k}^2 \quad (18)$$

$$\tilde{q}_{ij,k} = \sum_{g \in \mathcal{G}} \tilde{q}_{ij,k,g}, \quad \tilde{r}_{ij,k} = \sum_{g \in \mathcal{G}} R_g \tilde{\chi}_{ij,k,g} \quad (19)$$

$$\inf_{\Xi} \Pr \left\{ (1 - \gamma_{ij}) q_{ij}^{max} / 2 \leq [\tilde{q}_{ij,k}, \tilde{q}_{ij,k,g}] \leq (1 + \gamma_{ij}) q_{ij}^{max} / 2 \right\} \geq 1 - \epsilon^G \quad (20)$$

$$\inf_{\Xi} \Pr \left\{ p_i^{min} \leq \tilde{p}_{i,k} \leq p_i^{max} \right\} \geq 1 - \epsilon^G \quad (21)$$

where  $\tilde{p}_{i,k}$  is the gas pressure at bus  $i$  in time period  $k$ ;  $\gamma_{ij,k} = \text{sign}(q_{ij,k})$  is the direction of gas flow, where  $\text{sign}(\cdot)$  is the signal function;  $f_{ij}$ ,  $L_{ij}$ , and  $D_{ij}$  are the friction factor, length, and diameter of pipeline that connects bus  $i$  and  $j$ , respectively;  $\rho^{ng}$ ,  $T^{ng}$ , and  $z^{ng}$  are the gas density in standard temperature and pressure condition, temperature, compressibility factor of the gas mixture in the pipeline, respectively, which can be regarded as constants; the gas constant  $\tilde{r}_{ij,k}$ , on the contrary, is a variable changing with gas compositions;  $\tilde{q}_{ij,k}$  is the gas flow, and  $\tilde{q}_{ij,k,g}$  is the gas flow for gas component  $g$ ;  $R_g$  is the gas constant of gas component  $g$ ;  $q_{ij}^{max}$  is the transmission capacity of pipeline  $ij$ ;  $p_i^{min}$  and  $p_i^{max}$  are the lower and upper bounds for gas pressure, respectively.

During the transmission, the gases from different upstream pipelines and gas sources will be mixed uniformly, and then transported to downstream pipelines or other components. During this process, the following gas mixing equations and nodal balance equations in terms of different gas components should be followed:

$$\begin{aligned} \tilde{\chi}_{i,k,g} &= \left( \sum_{l \in \mathcal{L}_i^s} \tilde{q}_{i,l,k,g}^s + \sum_{l \in \mathcal{L}_i^{ptg}} \tilde{q}_{i,l,k,g}^{ptg} + \sum_{j \in \mathcal{J}_i} \frac{1 - \gamma_{ij}}{2} \tilde{q}_{ij,k,g} \right) \\ &/ \left( \sum_{l \in \mathcal{L}_i^s} \tilde{q}_{i,l,k}^s + \sum_{l \in \mathcal{L}_i^{ptg}} \tilde{q}_{i,l,k}^{ptg} + \sum_{j \in \mathcal{J}_i} \frac{1 - \gamma_{ij}}{2} \tilde{q}_{ij,k} \right) \end{aligned} \quad (22)$$

$$\tilde{q}_{ij,k,g} / \tilde{q}_{ij,k} = ((1 + \gamma_{ij}) \tilde{\chi}_{i,k,g} + (1 - \gamma_{ij}) \tilde{\chi}_{j,k,g}) / 2 \quad (23)$$

$$\begin{aligned} &\sum_{l \in \mathcal{L}_i^s} \tilde{q}_{i,l,k,g}^s + \sum_{l \in \mathcal{L}_i^{ptg}} \tilde{q}_{i,l,k,g}^{ptg} + \sum_{j \in \mathcal{J}_i} \frac{1 - \gamma_{ij}}{2} \tilde{q}_{ij,k,g} \\ &= \sum_{j \in \mathcal{J}_i} \frac{1 + \gamma_{ij}}{2} \tilde{q}_{ij,k,g} + \sum_{l \in \mathcal{L}_i^{gpp}} \tilde{q}_{i,l,k,g}^{gpp} + \tilde{q}_{i,k,g}^d \end{aligned} \quad (24)$$

where  $\mathcal{L}_i^s$ ,  $\mathcal{L}_i^{ptg}$ , and  $\mathcal{L}_i^{gpp}$  are the sets of gas sources, PTGs, and gas-fired power plants at bus  $i$ , respectively;  $J_i$  is the set of buses connected to bus  $i$ ;  $\tilde{q}_{i,l,k,g}^{gpp}$  is the gas consumption of gas component  $g$  for gas-fired power plant;  $\tilde{q}_{i,k,g}^d$  is the gas demand of gas component  $g$ .

For gas demand, though the gas composition varies, the supplied energy should equal to the requirement of the gas demand:

$$\sum_{g \in \mathcal{G}} GCV_g \tilde{q}_{i,k,g}^d = GCV^{ng} q_{i,k}^d \quad (25)$$

$$\tilde{q}_{i,k,g}^d / \sum_{g \in \mathcal{G}} \tilde{q}_{i,k,g}^d = \tilde{\chi}_{i,k,g} \quad (26)$$

where  $GCV^{ng}$  is the GCV of the natural gas;  $q_{i,k}^d$  is the gas demand measured by natural gas.

### C. Electricity system model

The operation of electricity systems is subject to the following generating unit constraints and electricity network constraints:

For  $l \in \mathcal{L}^{tpp}$ :

$$\inf_{\Xi} \Pr \left\{ P_{i,l}^{min} \leq \tilde{P}_{i,l,k} \leq P_{i,l}^{max} \right\} \geq 1 - \epsilon^E \quad (27)$$

For  $l \in \mathcal{L}^{gpp}$ :

$$\tilde{P}_{i,l,k} = \eta_{i,l}^{gpp} \sum_{g \in \mathcal{G}} \tilde{q}_{i,l,k,g} GCV_g \quad (28)$$

$$\tilde{q}_{i,l,k,g}^{gpp} / \sum_{g \in \mathcal{G}} \tilde{q}_{i,l,k,g}^{gpp} = \tilde{\chi}_{i,l,k,g} \quad (29)$$

$$\inf_{\Xi} \Pr \left\{ P_{i,l}^{min} \leq GCV^{ng} \tilde{q}_{i,l,k}^{gpp} \leq P_{i,l}^{max} \right\} \geq 1 - \epsilon^E \quad (30)$$

For  $l \in \mathcal{L}^{owf} \cup \mathcal{L}^{rng}$ :

$$\inf_{\Xi} \Pr \left\{ P_{i,l}^{min} \leq \tilde{P}_{i,l,k} \leq P_{i,l}^{max} \right\} \geq 1 - \epsilon^E \quad (31)$$

$$\sum_{l \in \mathcal{L}_i^{tpp} \cup \mathcal{L}_i^{gpp}} \tilde{P}_{i,l,k} - \sum_{l \in \mathcal{L}_i^{ptg}} \tilde{P}_{i,l,k}^{ptg} - P_{i,k}^d - \sum_{j \in \mathcal{J}_i} \tilde{P}_{ij,k} = 0 \quad (32)$$

$$\tilde{\theta}_{i,k} - \tilde{\theta}_{j,k} = X_{ij} \tilde{P}_{ij,k} \quad (33)$$

$$\inf_{\Xi} \Pr \left\{ -P_{ij}^{max} \leq \tilde{P}_{ij,k} \leq P_{ij}^{max} \right\} \geq 1 - \epsilon^E \quad (34)$$

where  $\mathcal{L}_i^{tpp}$ ,  $\mathcal{L}_i^{owf}$ , and  $\mathcal{L}_i^{rng}$  are the sets of traditional fossil power plants, OWFs, and other onshore renewable generators at bus  $i$ , respectively;  $\tilde{P}_{i,l,k}$  is the electricity generation of generator  $l$  at bus  $i$  in time step  $k$ ;  $P_{i,l}^{min}$  and  $P_{i,l}^{max}$  are the upper and lower bounds of the electricity generation of the generators, respectively;  $\eta_{i,l}^{gpp}$  is the efficiency of the gas-fired

power plant;  $P_{i,k}^d$  is electricity demands;  $\tilde{P}_{ij}$  is the electricity flow on branch  $ij$ ;  $\tilde{\theta}_i$  is the voltage angle at bus  $i$ ;  $X_{ij}$  is the reactance of branch;  $P_{ij}^{max}$  is the capacity of branch.

#### D. Objective function

Subject to the constraints above, the objective of our optimization problem is to minimize the day-ahead scheduling cost, and expected intraday operation cost under stochastic wind generations without violating constraints over a certain probability level. Then, the problem can be formulated as:

$$f = \min \sum_{k \in \mathcal{K}} \sum_{i \in \mathcal{I}} \mathbb{E}_{\Xi} \left( \sum_{l \in \mathcal{L}^{pp}} c_{i,l}^E \tilde{P}_{i,l,k} + \sum_{l \in \mathcal{L}^{gs}} c_{i,l}^G \tilde{q}_{i,l,k} \right) \quad (35)$$

where  $\mathcal{I}$  is the set of buses;  $c_{i,l}^E$  is cost coefficients of generators;  $c_{i,l}^G$  is the gas purchasing cost.

## V. SOLUTION METHOD

Due to the high nonconvexities, the DRCC problem formulated in the last section can not be solved tractably with off-the-shelf solvers in its current form. Therefore, the following reformulations and solution methods are tailored.

#### A. Reformulations of gas security chance constraints

The gas security constraints in (11) are double-side nonlinear joint constraints, which is challenging to handle. Therefore, we firstly use Taylor expansion to preliminarily approximate the Wobbe index constraints as in (36). Then, inner expressions of the Wobbe index in (11) can be converted into a linear form with respect to GCV and gas composition. Based on the structure of joint chance constraints, we separate it into multiple chance constraints based on Benferroni approximation theory [23], as shown in (37) (only left hand Wobbe index constraints are shown, the right hand side can be derived similarly).

$$WI_{i,k} = 2GCV_{i,k} \left( \sqrt{RD^{ng}} + RD_{i,k}/\sqrt{RD^{ng}} \right)^{-1} \quad (36)$$

$$\inf_{\Xi} \Pr \left\{ 2\sqrt{RD^{ng}} \sum_{g \in \mathcal{G}} \tilde{\chi}_{i,k,g} GCV_g - WI^{min,N} \right. \\ \left. \sum_{g \in \mathcal{G}} \tilde{\chi}_{i,k,g} RD_g \geq WI^{min,N} RD^{ng} \right\} \geq 1 - \epsilon^G/N^{jc} \quad (37)$$

where  $N^{jc}$  is the number of single constraints converted from the joint chance constraints.

Then, all inner expressions in the chance-constraints become linear. Generally, for the single/double sides chance constraints as in (38) and (39), they can be exactly reformulated into second order cone constraints as in (40) and (41), respectively [24].

$$\inf_{\Xi} \Pr \left\{ \mathbf{A}^T(\mathbf{x})\xi + \mathbf{B}(\mathbf{x}) \leq \mathbf{C} \right\} \geq 1 - \epsilon \quad (38)$$

$$\inf_{\Xi} \Pr \left\{ \left| \mathbf{A}^T(\mathbf{x})\xi + \mathbf{B}(\mathbf{x}) \right| \leq \mathbf{C} \right\} \geq 1 - \epsilon \quad (39)$$

$$\mathbf{A}^T(\mathbf{x})\mu + \mathbf{B}(\mathbf{x}) + ((1 - \epsilon)/\epsilon)^{\frac{1}{2}} \|\boldsymbol{\sigma}^{\frac{1}{2}}\mathbf{A}(\mathbf{x})\|_2 \leq \mathbf{C} \quad (40)$$

$$\begin{cases} u^2 + \left( \|\boldsymbol{\sigma}^{\frac{1}{2}}\mathbf{A}(\mathbf{x})\|_2 \right)^2 \leq (\mathbf{C} - v)^2 \epsilon \\ |\mathbf{B}(\mathbf{x})| \leq u + v, \quad u \geq 0, \quad 0 \leq v \leq \mathbf{C} \end{cases} \quad (41)$$

where  $\mathbf{A}(\mathbf{x})$  and  $\mathbf{B}(\mathbf{x})$  are the affine mapping of the wind forecast error ( $\mathbf{x}$  represents state variables);  $\mathbf{C}$  is right-hand side constant;  $u$  and  $v$  are two introduced ancillary variables. Then, all the chance constraints are reformulated into tractable forms.

#### B. Elimination of uncertainties in deterministic constraints

1) *For linear constraints*: Most of the constraints are linear, which can be written in the general form  $\mathbf{D}^T \tilde{\mathbf{x}} = \mathbf{E}$  for  $\forall \xi \in \Xi$ . Therefore, it can be equivalent to the following two constraints:

$$\mathbf{D}^T \mathbf{x} = \mathbf{E}, \quad \mathbf{D}^T \varphi = 0 \quad (42)$$

where  $\mathbf{D}$  and  $\mathbf{E}$  are coefficient matrices.

2) *For bilinear constraints*: Bilinear constraints appear in the gas mixing equations (22), (23), (26), and (29). They can be written in a general form  $\tilde{\mathbf{x}}^T \mathbf{F} \tilde{\mathbf{x}} + \mathbf{G}^T \tilde{\mathbf{x}} + \mathbf{H} = 0$ . With the similar idea in handling the linear constraints, it can be equivalent to:

$$\mathbf{x}^T \mathbf{F} \mathbf{x} + \mathbf{G}^T \mathbf{x} + \mathbf{H} = 0 \quad (43)$$

$$2\mathbf{x}^T \mathbf{F} \varphi + \mathbf{G}^T \varphi = 0, \quad \varphi^T \mathbf{F} \varphi = 0 \quad (44)$$

where  $\mathbf{F}$ ,  $\mathbf{G}$ , and  $\mathbf{H}$  are coefficient matrices. Note that thought  $\xi$  is eliminated from the formulation, it is still bilinear with respect to  $\mathbf{x}$  and  $\varphi$ . Then, sequential convex programming (SCP) method is used, which are introduced in the following subsections.

3) *For Weymouth equation with variant gas compositions*: Due to the variant gas compositions, the Weymouth equation (18) becomes a special form of cubic terms. Using second-order-cone relaxation and Taylor approximation, it can be split in to two second-order-cone/linear inequality constraints. Then, using similar formulations in (42) - (44), the chance constraints can be converted into deterministic constraints, and then be handled by SCP.

$$\tilde{p}_i^2 - \tilde{p}_j^2 \geq \Theta_{ij}(\hat{r}_{ij}\hat{q}_{ij}^2 + \tilde{r}_{ij}\hat{q}_{ij}^2 - \hat{r}_{ij}\hat{q}_{ij}^2) \quad (45)$$

$$\tilde{p}_i^2 - \tilde{p}_j^2 \leq \Theta_{ij}(\tilde{r}_{ij}\hat{q}_{ij}^2 + 2\hat{r}_{ij}\hat{q}_{ij}\tilde{q}_{ij} - 2\hat{r}_{ij}\hat{q}_{ij}^2) \\ + \varepsilon_{ij}, \quad \varepsilon_{ij} \geq 0 \quad (46)$$

where  $\Theta_{ij} = \gamma_{ij,k} \frac{16f_{ij}(\rho^{ng})^2 T^{ng} L_{ij} z^{ng}}{\pi^2 D_{ij}^5}$ ;  $(\hat{\cdot})$  is the reference value of variable  $(\cdot)$  in SCP, which will be specified in the next subsection;  $\varepsilon_{ij}$  is the slack variable. For all the detailed formulations in this Section, please find the supporting documents [25].

#### C. Solution procedures

The SCP-DRCC solution procedure is designed to solve the above nonconvex optimization problem. The idea is to solve deterministic optimization problem first, and then use the solution as references points for the DRCC problem to improve the computation efficiency. The detailed procedures are elaborated as follows:

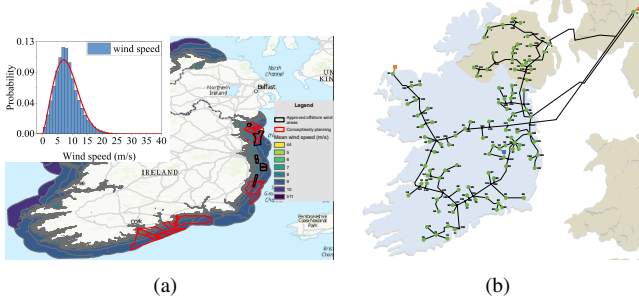


Fig. 5. Ireland Island energy systems: (a) OWF areas and wind speed distribution; (b) natural gas system. (Detailed schematic diagrams and data can be found on [25]).

**Step 1:** Calculate the moment-based ambiguity set for OWF generations according to the steps in Section III.

**Step 2:** Solve the deterministic optimal energy flow problem of H-IEGS according to [15]. Obtain the solution as reference point in iteration  $v = 0$ .

**Step 3:** In iteration  $v$  of the SCP, solve the reformulated DRCC problem (7)-(35), where the chance constraints and equality constraints are reformulated according to Section V.A and V.B, respectively. The bilinear terms are further reformulated by the following Taylor expansion (47), and objective function (35) are added with penalty terms as in (48). Then, the original intractable problem becomes second-order-cone programming problem, which can be solved directly by commercial solvers.

$$\hat{\mathbf{x}}^T \mathbf{J} \hat{\mathbf{x}} + \nabla(\mathbf{x}^T \mathbf{J} \mathbf{x})(\mathbf{x} - \hat{\mathbf{x}}) + \mathbf{K}^T \mathbf{x} + \mathbf{L} = 0 \quad (47)$$

$$\min f'^{(v)} = f + (\boldsymbol{\kappa}^{(v)})^T \boldsymbol{\varepsilon} \quad (48)$$

where  $\mathbf{J}$ ,  $\mathbf{K}$ , and  $\mathbf{L}$  are coefficient matrices; the reference point  $\hat{\mathbf{x}}$  is the solution of the optimization problem in last iteration  $v - 1$ ;  $\boldsymbol{\kappa}$  is the adaptive penalty factor.

**Step 4:** See if the convergence criterion is met, i.e.,  $|f'^{(v)} - f'^{(v-1)}| / (f'^{(v)} + f'^{(v-1)}) < \epsilon^{sp}$ . If yes, the solution in iteration  $v$  is the final solution; Otherwise, update penalty factor as  $\boldsymbol{\kappa}^{(v+1)} = \min\{\boldsymbol{\alpha}^T \boldsymbol{\kappa}^{(v)}, \boldsymbol{\kappa}^{max}\}$ , and start next iteration  $v + 1$  from **Step 3**. Then, we can obtain the final solution to the DRCC optimization problem.

## VI. CASE STUDIES

The electricity and gas systems on Ireland Island are used to validate the proposed method. As shown in Fig.5, the OWF are mainly under construction (or under conceptualization) in the east and south coastal areas, aiming for 5 GW capacity in 2030. The wind speed distributions, geographical outlines for OWF areas, and connection points are set according to [26]–[28]. The physical parameters of a 2 MW offshore WT model are used [6]. The Irish electricity transmission system has 1192 buses, 1369 branches, and 140 generators, with a total generating capacity of 19.55 GW [29]. The Irish gas system has 144 buses and 144 pipelines, with a total gas supply capacity of 41.21 Mm<sup>3</sup>/day [30].

### A. Validation of proposed SCP-DRCC method

In this subsection, the proposed SCP-DRCC is compared with other solution methods in terms of computation time,

TABLE I  
COMPARISONS OF DIFFERENT SOLUTION METHODS

Method	Method 1	Method 2	Method 3
Computation time (s)	0.9024	3.782	620.4
Objective function (€)	233527.87	233527.98	233527.86
Max relative differences	$2.97 \times 10^{-3}$	$1.49 \times 10^{-3}$	/

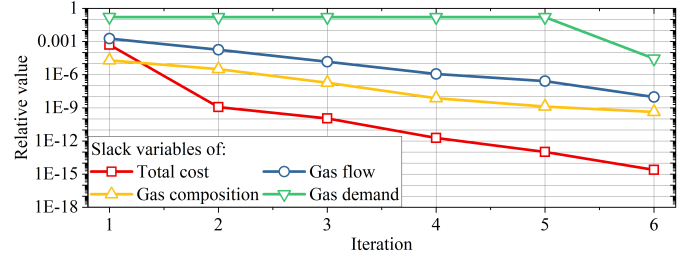


Fig. 6. Convergence of SCP-DRCC.

accuracy, and uncertainty handling. The optimization is performed on a laptop with AMD Ryzen 7 6800H CPU and 32 GB RAM.

**1) Computation time and accuracy:** Three methods are used to solve the nonconvex DRCC problem. Method 1 is the proposed SCP-DRCC; Method 2 uses the dynamic outer approximation technique to gradually approximate the bilinear constraints, which is built-in in Gurobi solver [31]; Method 3 uses a generally nonlinear solver IPOPT.

The comparisons of computation times, objective function values, and relative differences of representative state variables (hydrogen composition), are presented in Table. I. We can find that Method 1 has the best performance. Compared with the latest version (v11.0) of the quadratic solver in Gurobi, our algorithm improves the computation time by 76.14% in this optimization problem. Compared with the IPOPT, our algorithm even improves dramatically by 99.85%. According to the objective function values, the optimality of the three methods is very close. Regarding the relative difference in the solution of hydrogen composition, if we take the solution of IPOPT as the benchmark, our method is a little inferior to Method 2 but is totally acceptable. The differences are all below  $3 \times 10^{-3}$ . The convergence process is presented in Fig. 6. As we can see, it converges within six iterations, which is very fast considering the scale of the energy systems (thousands of buses).

**2) Handling of uncertainties:** Different solution methods for handling the uncertainty of offshore wind are compared. Method 4 is the proposed DRCC. Method 5 assumes the system operator knows the wind velocity perfectly in advance, and the deterministic solution method is used. Though it is merely possible in practice, it sets the lowest bounds for

TABLE II  
COMPARISON OF DIFFERENT UNCERTAINTY HANDLING METHODS

Method	Method 4	Method 5	Method 6
Total cost (€)	285791	281338	295053
Electricity system cost (€)	51917	56356	41287
Gas system cost (€)	233873	224982	253766
Electricity consumption of PTG (MW)	71.60	413.83	0
Hydrogen production of PTGs (Mm <sup>3</sup> /day)	0.4896	2.3588	0
Gas production of gas sources (Mm <sup>3</sup> /day)	26.88	25.87	29.14

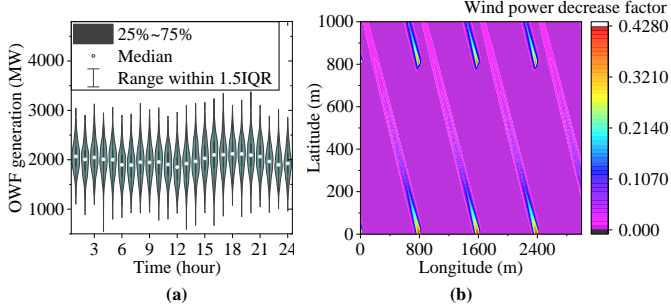


Fig. 7. (a) Wind speed in a typical day; (b) demonstration of wake effect.

operating cost as a reference; Method 6 uses the robust optimization framework, where the uncertainty budgets for OWFs are set to  $\pm\sigma$ .

The operational cost breakdown, as well as some key state variables in the three methods, are compared in Table II. We can find that our method achieves the best balance between cost and conservativeness. The risk level is  $\varepsilon = 0.05$  in Method 4, which can handle most of the stressed operation scenarios. Compared to the lowest cost in Method 5, the cost in Method 4 increases slightly by 1.58%, which is mainly reflected in the gas system cost (gas purchasing cost from gas sources). This is because due to the decrease of OWF capacity by considering the chance constraints, renewable hydrogen production from PTGs decreases by 79.24%. In contrast, Method 6 is more conservative. Its cost is 5.93% higher than in method 5, and the hydrogen production is zero. Therefore, it is not an appropriate operating strategy for energy system decarbonization.

#### B. Accommodation of offshore wind using hydrogen blending

In this case, three scenarios are considered based on Irish government policies for the future offshore wind development, and to validate the effectiveness of proposed hydrogen blending offshore wind accommodation scheme [32]. Scenario 1 considers the construction of 5GW offshore wind on the east coast, which is in line with Ireland's short-term goal in 2030. Scenario 2 reflects the mid-term goal in 2040 in the east and south coast areas, and the offshore wind capacity reaches 20 GW; In addition, Scenario 3 further extended offshore wind areas to Atlantic waters ocean, and trying to achieve 37 GW capacity in 2050. Two offshore wind accommodation schemes are used, including Scheme 1 using electricity system flexibility only, and Scheme 2 using hydrogen blending and natural gas system flexibility. Annual increases in power line capacity and electricity/gas demand are considered based on historical data [33].

The wind speed of each OWF area on a typical winter day is presented in Fig. 7. (a). The large volume of wind data puts heavy computation burdens on the calculation of the wake effect. By using our proposed recursive-tree-based calculation method and uncertainty modelling techniques, the number of scenarios required for wake effect calculation for one day can be reduced significantly from  $1.5 \times 10^8$  to 2524. Fig. 7. (b) visualize the wake effect of offshore turbines in an OWF area. The wind decrease factor denotes the percentage of decrease in wind speed after considering wake effects with

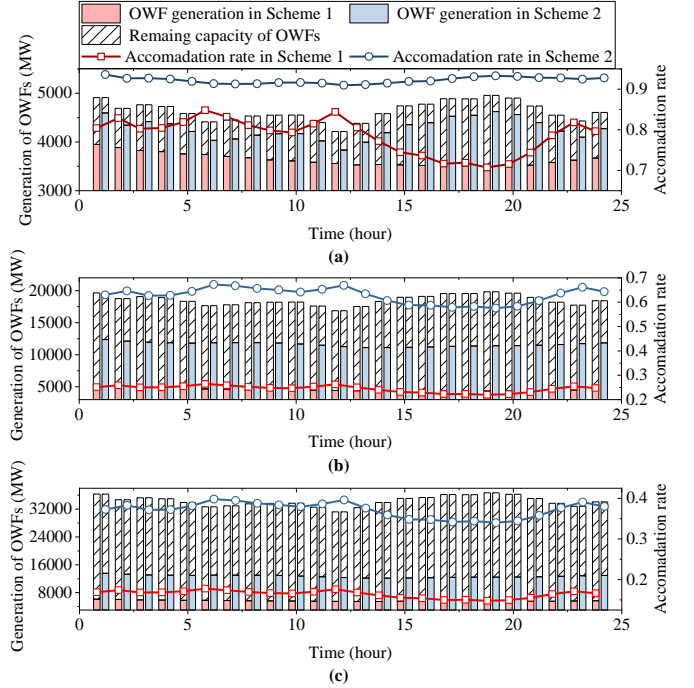


Fig. 8. OWF accommodation in: (a) 2030; (b) 2040; (c) 2050.

respect to the wind speed without wake effect. We can see that the wake effect is sparse and almost only affects the nearest downstream turbines, which demonstrates the necessity of using our method to avoid over-calculations.

The wind accommodation of OWFs in three scenarios using two schemes are presented in Fig. 8. We can find that the proposed hydrogen blending Scheme 2 can significantly promote the OWF accommodation rates in all three scenarios. In 2030, the average OWF accommodation rate on the typical day using Scheme 2 is 92.20%, which is 17.30% higher than Scheme 1. This trend becomes more apparent in 2040 and 2050, where the accommodation rates of Scheme 2 are 156.80% and 126.10% higher than those in Scheme 1. We can draw an important conclusion that the electricity system flexibility can be considered sufficient in accommodating the offshore goal of Ireland in 2030, but when the OWF capacity continues to grow in the long term, new technologies (such as hydrogen blending) are required. Nonetheless, we should also note that the absolute values of accommodation rates in Scheme 2 are also decreasing (in 2050, the accommodation rate in Scheme 2 is 37.15%), which needs further analysis in the next subsection.

To be aware of the gas system conditions and ensure its safety when using Scheme 2, the daily average hydrogen fractions across the network are presented in Fig. 9. We find that there is a clear line that separates the high hydrogen concentration areas and low hydrogen concentration areas. In the northeast areas is the upstream of the gas network with no offshore wind, and therefore the hydrogen is not blended. Since the hydrogen is blended in west Ireland from the Atlantic Ocean, east Dublin Bay, and South coastal areas, the hydrogen concentrations in southwest Ireland are relatively higher and reach their maximum possible value of 15.84% (constrained

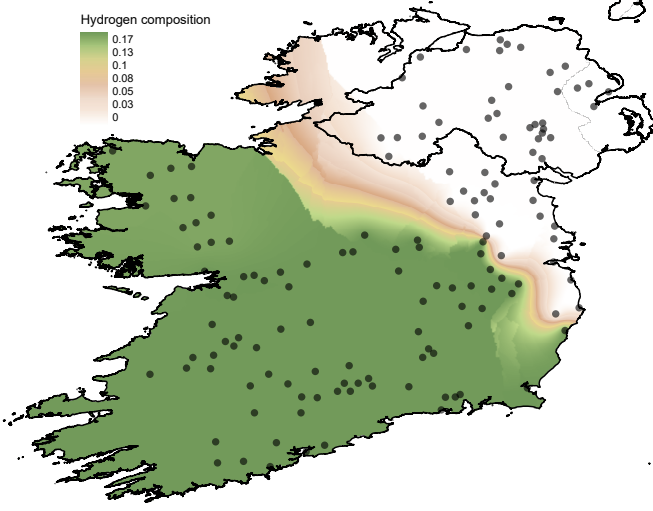


Fig. 9. Hydrogen composition distribution in Ireland Island gas network.

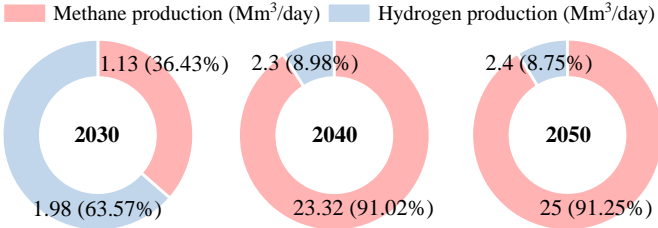


Fig. 10. Methane and hydrogen productions of PTGs in three scenarios.

by gas security limits). It is worth noting that although OWFs are interconnected to the Dublin area, due to the high load density, their electricity generations are consumed directly by electricity demand rather than converting into hydrogen, so the hydrogen concentration in the Dublin area is still low.

Though the hydrogen composition distribution in the three scenarios is identical, the offshore wind accommodation and PTG operating conditions are different, as summarized in Fig. 10. We can see that in 2030, most of the surplus offshore wind generation is used to produce hydrogen. While in 2040 and 2050 with the further increase in OWF capacity, the proportions of hydrogen productions are reduced significantly to only 9%. This is mainly because due to the gas security limits, the gas network is no longer able to absorb more hydrogen. This kind of decrease in hydrogen injection will lead to extra energy loss during the methanation process and higher carbon content in the gas network, and therefore is not beneficial for overall energy efficiency and decarbonization.

### C. Sensitivity analysis of technical advancements

Following the questions in the last subsection, we further investigate the impacts of different potential technical advancements on offshore wind accommodations in the future. Two pathways are assumed. In Pathway 1, we assume the system operator is able to predict the offshore wind with more accuracy, so the variance can be reduced; In Pathway 2, we assume technical modifications for gas system components and gas appliances have been (partially) completed, so the gas security constraints can be relaxed and higher fraction of

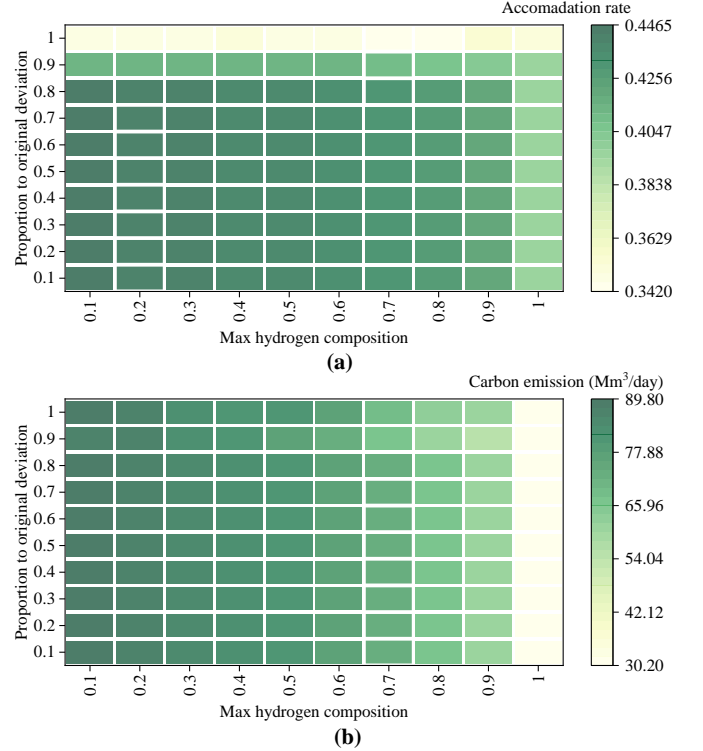


Fig. 11. Sensitivity analysis: (a) operational cost; (b) carbon emission.

hydrogen is allowed in the gas network. Sensitivity analysis is conducted for two pathways for the long-term Scenario 3.

The simulation results of offshore wind accommodation rate and carbon emission are shown in Fig. 11. It can be observed that both Pathways 1 and 2 affect these two aspects to different extents. The accommodation rate increases with the increase in wind prediction precision. However, we also notice that the positive impact of Pathway 1 has an upper limit even if the prediction precision increases to 100%. On the other hand, the advancement in Pathway 1 does not have significant impacts on reducing the system's carbon dioxide emissions.

It is worth noting that interestingly, the offshore wind accommodation rate will decrease slightly with the advancement in Pathway 2. This is because in the long-term scenario with 37 GW offshore wind capacity, even if the allowed hydrogen composition in the gas network is low, it can still be converted into methane and is sufficient to supply all the gas demands it can supply. In other words, when the offshore wind capacity is extremely large, the bottleneck would be the gas system transmission capacity rather than the maximum hydrogen composition. In this case, if the maximum allowed hydrogen composition increases, more hydrogen will be produced instead of methane. For example, when  $\sigma = 0.1\sigma_0$  and  $\chi^{hy,max} = 0.1$ , the total methane and hydrogen productions from PTGs are 25.41 and 1.48 Mm<sup>3</sup>/day, respectively. When  $\sigma = 0.1\sigma_0$  and  $\chi^{hy,max} = 1$ , the total methane and hydrogen productions from PTGs change to 4.59 and 63.00 Mm<sup>3</sup>/day, respectively. Due to the higher efficiency of hydrogen production, the offshore wind generation consumed by PTGs decreases, and therefore the accommodation rate decreases. Nonetheless, the system operating cost has been reduced from

269441 to 247376 €/hour, and the carbon dioxide emission also reduces significantly by 64.44%.

## VII. CONCLUSIONS

This paper proposes a novel framework to accommodate large-scale stochastic offshore wind by using the flexibility of hydrogen-blended electricity and gas systems, and the practical large-scale Ireland Island energy system is used to validate the proposed distributionally robust operation strategy. From the case studies, we validate that the proposed solution methods can improve the computation efficiency by 76.14% compared to the Gurobi solver. The Ireland government's ambitions on offshore wind in 2030/2040/2050 are analyzed. Compared with using electricity system flexibility only, our operating strategy can increase the offshore wind accommodation rate of the entire Ireland Island by up to 156.80%, and the hydrogen blending scheme is especially critical in the long-term future. Several potential technical advancements are analyzed, where 64.44% carbon emission could be reduced by using our operating strategy. We have also identified some barriers to offshore wind accommodation. Besides the hydrogen blending scheme, some supplementary measures, e.g., enhancing the gas system transmission capability, cross-border renewable electricity/gas trading, etc., are also critical for realizing Ireland Island's goal towards net zero in 2050.

## REFERENCES

- [1] Offshore wind energy capacity worldwide from 2009 to 2022. [Online]. Available: <https://www.statista.com/statistics/476327/global-capacity-of-offshore-wind-energy/>.
- [2] Policy statement on the framework for phase two offshore wind. [Online]. Available: <https://www.gov.ie/en/publication/f3bb6-policy-statement-on-the-framework-for-phase-two-offshore-wind/>.
- [3] M. Banzo and A. Ramos, "Stochastic optimization model for electric power system planning of offshore wind farms," *IEEE Transactions on Power Systems*, vol. 26, no. 3, pp. 1338–1348, 2010.
- [4] C. Lin, Z. Bie, and C. Chen, "Operational probabilistic power flow analysis for hybrid ac-dc interconnected power systems with high penetration of offshore wind energy," *IEEE Transactions on Power Systems*, 2022.
- [5] P. Hou, W. Hu, M. Soltani, C. Chen, B. Zhang, and Z. Chen, "Offshore wind farm layout design considering optimized power dispatch strategy," *IEEE Transactions on Sustainable Energy*, vol. 8, no. 2, pp. 638–647, 2016.
- [6] S. Tao, S. Kuenzel, Q. Xu, and Z. Chen, "Optimal micro-siting of wind turbines in an offshore wind farm using frandsen-gaussian wake model," *IEEE Transactions on Power Systems*, vol. 34, no. 6, pp. 4944–4954, 2019.
- [7] S. Paul, A. P. Nath, and Z. H. Rather, "A multi-objective planning framework for coordinated generation from offshore wind farm and battery energy storage system," *IEEE Transactions on Sustainable Energy*, vol. 11, no. 4, pp. 2087–2097, 2019.
- [8] S. Tao, Q. Xu, A. Feijóo, and G. Zheng, "Joint optimization of wind turbine micrositing and cabling in an offshore wind farm," *IEEE Transactions on Smart Grid*, vol. 12, no. 1, pp. 834–844, 2020.
- [9] X. Guo, X. Chen, X. Chen, P. Sherman, J. Wen, and M. McElroy, "Grid integration feasibility and investment planning of offshore wind power under carbon-neutral transition in china," *Nature Communications*, vol. 14, no. 1, p. 2447, 2023.
- [10] Hydeploy. [Online]. Available: <https://hydeploy.co.uk/>.
- [11] Hyblend: Opportunities for hydrogen blending in natural gas pipelines. [Online]. Available: <https://www.energy.gov/eere/fuelcells/hybrid-opportunities-hydrogen-blending-natural-gas-pipelines>.
- [12] I. Saedi, S. Mhanna, and P. Mancarella, "Integrated electricity and gas system modelling with hydrogen injections and gas composition tracking," *Applied Energy*, vol. 303, p. 117598, 2021.
- [13] S. Zhang, S. Wang, Z. Zhang, J. Lyu, H. Cheng, M. Huang, and Q. Zhang, "Probabilistic multi-energy flow calculation of electricity–gas integrated energy systems with hydrogen injection," *IEEE Transactions on Industry Applications*, vol. 58, no. 2, pp. 2740–2750, 2021.
- [14] A. De Corato, I. Saedi, S. Riaz, and P. Mancarella, "Aggregated flexibility from multiple power-to-gas units in integrated electricity-gas-hydrogen distribution systems," *Electric Power Systems Research*, vol. 212, p. 108409, 2022.
- [15] S. Wang, J. Zhai, and H. Hui, "Optimal energy flow in integrated electricity and gas systems with injection of alternative gas," *IEEE Transactions on Sustainable Energy*, 2023.
- [16] Y. Qiu, S. Zhou, W. Gu, Y. Lu, X.-P. Zhang, G. Han, K. Zhang, and H. Lv, "Network modeling and operation optimization of electricity-hydrogen-integrated energy system," *CSEE Journal of Power and Energy Systems*, 2023.
- [17] Y. Jiang, Z. Ren, Z. Y. Dong, Z. Sun, and V. Terzija, "An optimal dispatch method of integrated electricity and gas systems incorporating hydrogen injection flexibility," *International Journal of Electrical Power & Energy Systems*, vol. 155, p. 109662, 2024.
- [18] P. Zhao, C. Gu, Z. Hu, D. Xie, I. Hernando-Gil, and Y. Shen, "Distributionally robust hydrogen optimization with ensured security and multi-energy couplings," *IEEE Transactions on Power Systems*, vol. 36, no. 1, pp. 504–513, 2020.
- [19] The gas safety (management) (amendment) (no. 2) regulations 2023. [Online]. Available: <https://www.legislation.gov.uk/uksi/2023/320/contents/made>.
- [20] L. Yang, Y. Xu, W. Gu, and H. Sun, "Distributionally robust chance-constrained optimal power-gas flow under bidirectional interactions considering uncertain wind power," *IEEE Transactions on Smart Grid*, vol. 12, no. 2, pp. 1722–1735, 2020.
- [21] L. Yang, Y. Xu, J. Zhou, and H. Sun, "Distributionally robust frequency constrained scheduling for an integrated electricity-gas system," *IEEE Transactions on Smart Grid*, vol. 13, no. 4, pp. 2730–2743, 2022.
- [22] M. Bao, Y. Ding, C. Shao, Y. Yang, and P. Wang, "Nodal reliability evaluation of interdependent gas and power systems considering cascading effects," *IEEE Transactions on Smart Grid*, vol. 11, no. 5, pp. 4090–4104, 2020.
- [23] A. Nemirovski and A. Shapiro, "Convex approximations of chance constrained programs," *SIAM Journal on Optimization*, vol. 17, no. 4, pp. 969–996, 2007.
- [24] H. Li, Q. Wu, L. Yang, H. Zhang, and S. Jiang, "Distributionally robust negative-emission optimal energy scheduling for off-grid integrated electricity-heat microgrid," *IEEE Transactions on Sustainable Energy*, 2023.
- [25] Github repositories. [Online]. Available: <https://github.com/ShengWang-EE/J-offshore-wind-hydrogen>.
- [26] Presence of wind farm sites in irish waters. [Online]. Available: <https://data.gov.ie/dataset/presence-of-wind-farm-sites-in-irish-waters>.
- [27] Mean offshore wind speed 2003 - height 50m above mean sea level. [Online]. Available: <https://data.gov.ie/dataset/mean-offshore-wind-speed-2003-height-50m-above-mean-sea-level>.
- [28] East coast generation opportunity assessment. [Online]. Available: <https://www.eirgridgroup.com/site-files/library/EirGrid/East-Coast-Generation-Opportunity-Assessment.pdf>.
- [29] All-island ten-year transmission forecast statement. [Online]. Available: <https://www.eirgridgroup.com/site-files/library/EirGrid/All-Island-Ten-Year-Transmission-Forecast-Statement-TYTF-2021.pdf>.
- [30] Network development plan. [Online]. Available: <https://www.gasnortworks.ie/docs/corporate/gas-regulation/GNI-2021-Network-Development-Plan.pdf>.
- [31] What's new in gurobi 11.0. [Online]. Available: <https://cdn.gurobi.com/wp-content/uploads/Whats-New-in-Gurobi-11.0-Webinar-slides.pdf?x34984>.
- [32] Policy statement on the framework for phase two offshore wind. [Online]. Available: <https://www.gov.ie/en/publication/f3bb6-policy-statement-on-the-framework-for-phase-two-offshore-wind/>.
- [33] Electricity. [Online]. Available: <https://www.seai.ie/data-and-insights/seai-statistics/key-statistics/electricity/>.